INSTITUTE FOR FUSION STUDIES

DOE/ET-53088-527 IFSR #527

Toroidal Kinetic η_i-mode Study in High Temperature Plasmas

J.Q. DONG,[a] W. HORTON, and J.Y. KIM
Institute for Fusion Studies
The University of Texas at Austin
Austin, Texas 78712

November 1991

[a] *Permanent address: Southwestern Institute of Physics, Leshan, China*

THE UNIVERSITY OF TEXAS

AUSTIN

Toroidal Kinetic η_i-mode Study in High Temperature Plasmas

J.Q. Dong,[a] W. Horton, and J.Y. Kim
Institute for Fusion Studies
The University of Texas at Austin
Austin, Texas 78712

Abstract

A new kinetic integral equation for the study of the ion temperature gradient driven mode in toroidal geometry is developed that includes the ion toroidal (curvature and magnetic gradient) drift motion ω_D, the mode coupling from finite $k_\parallel$ due to the toroidal feature of the sheared magnetic configuration. The integral equation allows the stability study for arbitrary $k_\parallel v_i/(\omega - \omega_D)$ and $k_\perp \rho_i$. A systematic parameter study is carried out for the low β circular flux surface equilibrium. Possible correlations between the unstable mode characteristics and some experimental results such as fluctuation spectrum and anomalous ion transport measurements are discussed.

[a]Permanent address: Southwestern Institute of Physics, Leshan, China

I. Introduction

The ion temperature gradient driven mode (ITG mode), or η_i-mode, has been of great interest in theoretical studies of plasma confinement physics and nuclear fusion in recent years. The objectives of these investigations are to understand and to explain some experimental observations which indicate that the η_i-mode turbulence is a plausible candidate for the anomalous ion energy transport.[1-4] Some fluctuation studies[5,6] suggest the presence of the ion-mode feature, but a direct correlation of such turbulence with theory on the anomalous ion transport has not been obtained.

A comprehensive study[7] on the correlation between the η_i-mode turbulence and the density modification experiment on the TFTR tokamak is carried out, recently, with existing η_i-mode theories. It is pointed out[7] that present theories seem to be insufficient to explain some experimental observations and a more complete study of η_i-mode is anticipated. Here an improved formalism for the most general integral equation for low frequency perturbations such as the η_i-mode in toroidal geometry derived in Ref. 8 is developed and applied to obtain detailed numerical results for tokamak plasma parameters.

Theoretical studies on η_i-mode are numerous. Most of the studies, however, are performed under some limits or approximations. The slab η_i-mode studies[9-11] only consider the driving force due to the coupling of the parallel transit of the particles with the temperature gradient. The kinetic effects including the arbitrary Larmor radius effect and the full parallel Landau resonance damping are taken into account while the particle drift motion due to magnetic curvature and gradient are neglected. In the fluid limit[12-14] these kinetic effects are neglected where some nonlinear studies are carried out due to the simplicity of the equations used. Local toroidal η_i-mode studies[15,16] consider the driving force due to the coupling of the particle curvature and grad-B drift with temperature gradient while neglecting the variation of the drift motion along the poloidal direction and shear effect. Some expansions[17,18] such

as small $k_{\|}v_i/(\omega - \omega_D)$ can significantly reduce the complexity of the gyrokinetic equation in toroidal geometry but are not appropriate when such conditions are broken. An integral equation including all ion kinetic mechanisms except the trapped particle effect is derived in Ref. 8 but emphasis is put on the fluid and local kinetic limits and very few results are available in the general kinetic parameter regime. A comprehensive study of the η_i-mode is carried out in Ref. 19 using a particle simulation approach.

A more complete study of the η_i-mode in toroidal geometry is needed either in order to more accurately asses the actual relevance of the η_i-mode to the experimental observations or for the completeness of η_i-mode theoretical study.

In the present work we derive a new integral equation to study the ion temperature gradient driven mode in toroidal geometry. This equation includes the curvature and magnetic gradient drift motion of the ions and the mode coupling due to the spatial inhomogeneity in the toroidal magnetic configuration. The full ion transit $k_{\|}v_{\|}$ and toroidal drift effects $\omega_D(v_{\perp}^2, v_{\|}^2, \theta)$ are retained while the ion bouncing motion is neglected for simplicity. Electrons are considered to be adiabatic. Essentially, the new equation is equivalent to the one derived in Ref. 8. Nevertheless the integral equation given in the present work has some characteristics which allow the fast computation of the spectrum of eigenvalues with the modest computer time (3 min/eigenvalue on the CRAY-2). By using the integral equation, detailed full kinetic results for a number of issues such as the effects of toroidicity, safety factor, shear, and the ratio of the electron temperature to the ion temperature on the mode are obtained. At the same time a quasi-toroidal model is considered where the magnetic curvature and grad-B drift is assumed to be constant over a flux surface (a more detailed explanation is given in Sec. II). Results from the general toroidal equation, the quasi-toroidal model and the familiar local kinetic equation are compared.

The remainder of this work is organized as follows. In Sec. II the new integral equation is given and its characteristics are discussed. The numerical results are presented and compared

in Sec. III, and the concluding remarks and discussions are given in Sec. IV.

II. Integral Equation in Toroidal Geometry

The dynamics of a low frequency electrostatic perturbation in inhomogeneous plasmas is described by the quasineutrality condition,

$$\tilde{n}_e = \tilde{n}_i \ . \tag{1}$$

Here, in the η_i mode study the perturbed electron density $\tilde{n}_e$ is taken to be the adiabatic response to the electrostatic perturbation $\tilde{\phi}$; i.e,

$$\tilde{n}_e = \frac{en_{0e}}{T_e}\tilde{\phi} \ . \tag{2}$$

On the other hand, the perturbed ion density $\tilde{n}_i$ in an axisymmetric toroidal geometry (like tokamak) is given by

$$\tilde{n}_i = -\frac{en_{0i}}{T_i}\tilde{\phi} + \int d^3v J_0(\alpha) h \ , \tag{3}$$

where T_e and T_i are the temperature of the electrons and the ions respectively, and $\alpha = (2b_i)^{1/2} v_\perp$, $v = v/v_{ti}$, $2b_i = k_\perp^2 v_{ti}^2/\Omega_i^2$, $v_{ti} = (2T_i/m_i)^{1/2}$, and $\Omega_i = eB/m_i c$ is the ion gyrofrequency, $J_0(\alpha)$ the Bessel function of zeroth order. The nonadiabatic response h is determined by solving the gyro-kinetic equation,

$$i\frac{v_\parallel}{Rq}\frac{\partial}{\partial\theta}h + (\omega - \omega_D)h = (\omega - \omega_{*T})J_0(\alpha)F_M\frac{en_{0i}}{T_i}\hat{\phi}(\theta) \tag{4}$$

with

$$\omega_D = 2\tau_e^{-1}\epsilon_n\omega_{*e}(\cos\theta + \hat{s}\theta\sin\theta)\left(\frac{v_\perp^2}{2} + v_\parallel^2\right) \tag{5}$$

where $\omega_{*T} = -\tau_e^{-1}\omega_{*e}\left[1 + \eta_i\left(v_\perp^2 + v_\parallel^2 - \frac{3}{2}\right)\right]$, $\omega_{*e} = \frac{ck_\theta T_e}{eBL_n}$ is the electron diamagnetic drift frequency, $L_n = -(d\ell n\, n/dr)^{-1}$ is the density gradient scale length; $\eta_i = L_n/L_{Ti}$ with L_{Ti} being the ion temperature gradient scale length; $\epsilon_n = \frac{L_n}{R}$ with R being the major

radius of the torus; $\tau_e = \frac{T_e}{T_i}$; the magnetic shear $\hat{s} = \frac{r}{q}\frac{dq}{dr}$ with q being the safety factor; $F_M = (\pi v_{ti}^2)^{-3/2}\exp(-v^2)$. We note that the well-known ballooning mode representation[20]

$$\tilde{f}_n(r,\theta,\zeta) = \sum_{m=-\infty}^{\infty} e^{im\theta}\int_{-\infty}^{\infty} e^{-im\theta'}e^{-in(\zeta-q\theta')-i\omega t}\hat{f}_n(\theta')d\theta' \ , \tag{6}$$

where ζ and θ are the toroidal and the extended poloidal angle, respectively, has been used in deriving Eq. (4) and the usual circular flux surface equilibrium model has been used in Eq. (5).

In solving Eq. (4), for simplicity, we ignore the trapped ion contribution, which is relevant only for very low frequency perturbations of $\omega \simeq \omega_{bi}$ (ion bounce frequency). In addition for the passing particles we neglect the $v_{||}$ modulation along the unperturbed particle orbit due to the equilibrium magnetic field. The following Fredholm homogeneous integral equation of second kind[21] can be obtained from the quasineutrality condition Eq. (1),

$$(1+\tau_e)\hat{\phi}(\theta) = \int_{-\infty}^{+\infty} d\theta' \, K(\theta,\theta')\hat{\phi}(\theta') \tag{7}$$

with

$$K(\theta,\theta') = -i\tau_e\int_0^{\infty} 2\pi v_\perp dv_\perp \int_0^{\infty} dv_{||}\,\frac{qR}{|v_{||}|}\,e^{i(\sigma(\theta)-\sigma(\theta'))\mathrm{sgn}(\theta-\theta')}\,(\omega-\omega_{*T})J_0(\alpha)J_0(\alpha')F_M \tag{8}$$

where

$$\sigma(\theta) = \int^{\theta} d\theta''\frac{qR}{|v_{||}|}\,(\omega-\omega_D(\theta'')) \tag{9}$$

and the nonadiabatic response h, the solution of Eq. (4) with the boundary condition $h(\theta)=0$ as $|\theta|\to\infty$,[8] has been obtained and substituted into Eq. (3). The $v_\perp$ integration in Eq. (8) can be performed analytically, and the resulting equation is the Eq. (7) of Ref. 8.

A. Toroidal Kinetic Integral Equation

In contrast to Ref .8 the $v_{||}$ integration in Eq. (8) is changed to the integration over τ by introducing

$$\tau = \frac{qR|\theta-\theta'|}{v_{||}v_{ti}} \ . \tag{10}$$

It is easy to recognize that τ is the time interval $t - t'$ with t and t' being the time corresponding to the extended poloidal positions θ and θ', respectively, in the present case that the modulation of $v_{\|}$ along unperturbed particle orbit is neglected. Now it is the right time to point out that the kernel of the integral equation is the ensemble average over the Maxwellian velocity of the two-time $t - t' = \tau$ correlation function required for the nonlocal plasma susceptibility operator $\widehat{\chi}_j$ defined by $\delta n_j(\mathbf{x}, \mathrm{t}) = (\mathrm{n_{0j}e_j/T_j})\widehat{\chi}_\mathrm{j}\phi(\mathbf{x}', \mathrm{t}')$. The integration over $v_\perp$ in Eq. (8) is carried out by taking advantage of the collisionless phase mixing that occurs from the velocity dispersion in the grad-B drift and the result gives the power law decay in τ of the integral operator. Thus for large $\omega_D\tau$, corresponding to small ω/ω_D, the correlation function decays as $1/(\tau\omega_D)^{3/2}$ (see Eq. (12) below) even for $k_{\|} = 0$, where the usual transit time phase mixing $\exp(-k_{\|}^2 v_T^2 \tau^2)$ vanishes. For small τ the expansion of Eq. (7) leads to the usual small ω_D/ω fluid regime. We also use the dimensionless variable $k = \widehat{s}(r_0)k_\theta\theta = \widehat{s}(r_0)m/r_0\theta$, which is the Fourier transform of the radial variable $x = r - r_0$ (r_0 being defined by $q(r_0) = m/n$) in the toroidal model given by Eq. (6). The connection between $k = k_x\rho_s$ and the ballooning variable θ is derived by expanding the phase factor $\exp(inq(r)\theta')$ in Eq. (6) about the local nearest rational surface. By introducing such conversion from θ's to k's the integral equations (7) and (8) now can be written as

$$(1 + \tau_e)\widehat{\phi}(k) = \int_{-\infty}^{+\infty} \frac{dk'}{\sqrt{2\pi}} K(k, k')\widehat{\phi}(k') \tag{11}$$

with

$$K(k, k') = -i \int_{-\infty}^{0} \omega_{*e}\, d\tau \frac{\sqrt{2}\, e^{-i\omega\tau}}{\sqrt{a}(1+a)\sqrt{\lambda}} e^{-(k-k')^2/4\lambda} \left\{ \frac{\omega}{\omega_{*e}} \tau_e + 1 - \frac{3}{2}\eta_i \right.$$

$$\left. + \frac{2\eta_i}{(1+a)} \left[1 - \frac{k_\perp^2 + k_\perp'^2}{2(1+a)\tau_e} + \frac{k_\perp\, k_\perp'}{(1+a)\tau_e} \frac{I_1}{I_0} \right] + \frac{\eta_i(k-k')^2}{4a\lambda} \right\} \Gamma_0(k_\perp, k_\perp') \,, \tag{12}$$

where

$$\lambda = \frac{\tau^2}{\tau_e a} \left(\frac{\widehat{s}}{q} \epsilon_n \right)^2 \omega_{*e}^2 a = 1 + \frac{i2\epsilon_n}{\tau_e} \omega_{*e}\tau \left\{ \frac{[(\widehat{s}+1)(\sin\theta - \sin\theta') - \widehat{s}(\theta\cos\theta - \theta'\cos\theta')]}{(\theta - \theta')} \right\} \tag{13}$$

$$\theta = \frac{k}{\widehat{s}\, k_\theta}, \qquad \theta' = \frac{k'}{\widehat{s}\, k_\theta}\ , \tag{14}$$

$$\Gamma_0 = I_0\left(\frac{k_\perp\, k'_\perp}{\tau_e(1+a)}\right) e^{-(k_\perp^2+k_\perp'^2)/2\tau_e(1+a)}\ , \tag{15}$$

$$k_\perp^2 = k_\theta^2 + k^2\ , \qquad k_\perp'^2 = k_\theta^2 + k'^2\ , \tag{16}$$

and $I_j(j=0,1)$ is the modified Bessel function of order j. Also, the wave numbers k_θ, k and k' are normalized to ρ_s^{-1} with $\rho_s = \sqrt{\frac{2T_e}{m_i}}/\Omega_i$.

B. Quasi-Toroidal Kinetic Integral Equation

By looking at the Eqs. (5) and (14) it is easy to notice that the nonlocal contribution of $\omega_D(\theta)$ in Eq. (5), $(\cos\theta + \widehat{s}\theta sin\theta)$, appears in the second term of Eq. (14) on the right side as the average of ω_D (Eq. (5)) over the region (θ',θ). If we choose $\theta = 0$ in Eq. (5), which means that the magnetic curvature and grad-B drifts are considered to be constant and equal to the maximum value at $\theta = 0$, then we get the following integral equation for quasi-toroidal model,[22]

$$(1+\tau_e)\widehat{\phi}(k) = \int_{-\infty}^{+\infty} \frac{dk'}{\sqrt{2\pi}} K(k,k')\widehat{\phi}(k') \tag{17}$$

with

$$K(k,k') = -i\int_{-\infty}^{0} \omega_{*e}\, d\tau\, \frac{\sqrt{2}\, e^{-i\omega\tau}}{\sqrt{a}\,(1+a)\sqrt{\lambda}}\, e^{-(k-k')^2/4\lambda} \left\{ \frac{\omega}{\omega_{*e}}\tau_e + 1 - \frac{3}{2}\eta_i \right.$$

$$\left. + \frac{2\eta_i}{(1+a)}\left[1 - \frac{k_\perp^2 + k_\perp'^2}{2(1+a)\tau_e} + \frac{k_\perp\, k'_\perp}{(1+a)\tau_e}\frac{I_1}{I_0}\right] + \frac{\eta_i(k-k')^2}{4a\lambda} \right\} \Gamma_0(k_\perp, k'_\perp)\ , \tag{18}$$

where

$$\lambda = \frac{\tau^2}{\tau_e a}\left(\frac{L_n}{L_s}\right)^2 \omega_{*e}^2 \tag{19}$$

$$a = 1 + \frac{i2\epsilon_n}{\tau_e}\omega_{*e}\tau\ , \tag{20}$$

and L_s is the scale length of the magnetic shear. All remaining expressions are the same as in the toroidal kinetic integration case. If we put $\epsilon_n = 0$ in Eq. (18) then it reduces to the sheared slab η_i mode integral equation.[10] On the other hand, if $\widehat{\phi}(k) = \text{const.}$ corresponding to $\widetilde{\phi}(x) \sim \delta(x - x')$, then the k' integration can be done and Eq. (18) reduces to the local kinetic dispersion relation.[16]

Essentially, equation (11) is equivalent to Eq. (5) of Ref. 8 (will be referred to as Romanelli equation hereafter). However, Eq. (11) has some characteristics compared with Romanelli equation.

First, Eq. (11) shows more clearly the relation between the sheared slab and the toroidal modes. This is due to the change of the ballooning mode space variable θ to k which corresponds to the Fourier transform of the real space variable x in sheared slab limit. In addition, in Eq. (11) it is easy to identify the shear effect and ballooning effect which are both considered to be important in toroidal geometry. In a general toroidal geometry, where the eigenvalue equation is a complicated 2-dimensional equation in the r, θ space, we may consider that $k_{||}$ decomposes into $k_{||} = k_{||}^{(t)} + k_{||}^{(s)}$, where $k_{||}^{(t)}$ and $k_{||}^{(s)}$ stand for the ballooning contribution to $k_{||}$ (from the variation of the poloidal modulation in θ direction of the equilibrium) and magnetic shear contribution to $k_{||}$ (from the variation of the direction of the magnetic field with r), respectively. In the well-known ballooning mode formalism for the toroidal mode, the shear effect $k_{||}^{(s)}$ is obtained from the twisting of the eikonal phase factor in Eq. (6) which locally varies as $e^{inq'\theta x}$ for the radial profile of the eigenfunction to reduce the 2-D problem to 1-D problem. Effectively, with this local expansion the ballooning mode formalism emphasizes the exact treatment of the ballooning structure of the eigenfunction and the toroidal curvature and the magnetic gradient drifts, i.e. the ballooning effect, while admits a poor treatment of the local shear and the global radial structure of the eigenmode. To treat the local shear effect and the global structure of the mode more exactly, an alternative approximate method has, recently, been used in the fluid simulation

study by Hong and Horton.[22] This method[22] assumes that the toroidal driving force is a constant over a flux surface without variation along the poloidal angle θ, so that $k_{\|}^{(t)} \simeq 0$. The toroidal driving force is taken to be the local maximum value at the point $\theta = 0$, so that $\omega_D \simeq k_y v_D = 2\epsilon_n \omega_* (v_\perp^2/2 + v_{\|}^2)$. While this model[22] makes it possible to do the non-linear simulation of the toroidal mode, we show here that in the long wavelength regime $k_\theta \rho_s \sim \epsilon_n/q$ it overestimates the growth rate by a factor of 2.

In the quasi-toroidal model (Eq. (18)) the same approach as in Ref. 22 is used for the kinetic study of the η_i-mode. In this model the eigenvalue equation takes the same form as the sheared slab model, except the toroidal mode driving force, which is assumed to be uniform over a flux surface, has been included. So that this model emphasizes the shear effect and ignores the ballooning effect while both approaches keep the toroidicity induced drift effect which is the most important driving force in toroidal geometry.

The second difference of our equation from the Romanelli equation is that the numerical calculation of the eigenvalue can be performed more efficiently than using the Romanelli equation. This is because, first, the kernel $K(k, k')$ of Eq. (11) as given in Eq. (12) vanishes as $e^{-(k-k')^2}$ when $(k - k')$ increases while the kernel of Romanelli equation vanishes as $e^{-(\chi - \chi')}$ when $(\chi - \chi')$ increases, (χ in Romanelli equation is the extended poloidal angle as θ in Eq. (11)). Second, the kernel of Romanelli equation oscillates very rapidly due to the large phase factor in Eq. (8), $\sigma(\theta) - \sigma(\theta')$, when $v_{\|} \to 0$ and $(\chi - \chi')$ is small but not zero. The oscillation characteristics of the kernel in Eq. (11) do not change when $\tau \to 0$ and $(k - k')$ is small but not zero. Here by changing the $v_{\|}$ integration to τ integral the phase mixing of the oscillation is taken into account analytically leaving the rapid convergent kernel. It is these differences that make the matrix obtained from Eq. (11) a more nearly diagonal matrix which improves the numerical representation of the integral operator and allows the eigenvalue problem to converge much faster. Our numerical experience has shown that the computer time needed to study toroidal η_i-mode with Eq. (11) is about half that required

for the Romanelli equation.

Finally the local kinetic dispersion relation,[16]

$$(1+1/\tau_e) = \int d^3v \frac{(\omega-\omega_{*T})J_0^2(\alpha)F_M}{\omega-\omega_D-k_{\|}v_{\|}} \tag{21}$$

can be easily obtained from Eq. (4) by taking $\frac{1}{Rq}\frac{\partial}{\partial\theta} = ik_{\|}$ and $\omega_D(\theta) = \omega_D(0)$. Eq. (22) also follows from Eq. (18) by taking $\widehat{\phi}(k) = \text{const.}$ and doing the k' integral.

III. Numerical Results

A computer code is developed to solve Eq. (11) numerically. At $k = k'$ the kernel has a logarithmic singularity which can be easily handled by standard techniques as pointed out in Ref. 8. The integration over τ in Eq. (12) is performed with Gaussian rule of even order. The integration over k' in Eq. (11) is carried out with rectangle rule except near $k' = k$ where the Gaussian rule of even order is used.

The computer code is tested in two ways. First, it is run in the sheared slab limit ($\epsilon_n = 0$) and tested with the results given in Ref. 10. Second, for $\eta_i = 2.5$, $\widehat{s} = q = \tau = 1$, $k_\theta\,\rho_s = 0.45$, $\epsilon_n = 0.25$ the normalized real frequency $\Omega_r = \omega_r/\omega_{*e} = -0.607$ and growth rate $\Omega_i = \gamma/\omega_{*e} = 0.258$ are obtained for toroidal mode. The growth rate agrees well with the result given in Ref. 8 while the real frequency is not available there.

In general the dimensionless complex eigenvalue Ω is a function of the six parameters η_i, ϵ_n, τ, $\widehat{s}$, q, k_θ. We have recorded and tabulated the Ω's from all cases that we have run in a data base to be made available in a NERSC public domain file.

1. η_i and $k_\theta\rho_s$ variation

The normalized growth rate and real frequency as a function of η_i are given in Fig. 1 for $T_e/T_i = 1$, $k_\theta\rho_s = 0.75$, $L_n/L_s = 0.1$ and $\epsilon_n = 0.2$. The solid lines are from Eq. (11) of ballooning formalism and the dotted lines are the results from Eq. (18) of the quasi-toroidal

model. The parameters $\hat{s}$ and q for Eq. (11) are chosen such that $L_n/L_s = \hat{s}\epsilon_n/q = 0.1$, ($q = 2$, $\hat{s} = 1$). As a comparison the results for slab with the same parameters are given in Fig. 1 by the $\epsilon_n = 0$ curves. For $\epsilon_n = 0.2$ and 0.4 we find that there is a good agreement between full Eq. (11) and the quasi-toroidal model in the growth rate and the real frequency.

In Fig. 2 we show the eigenfunctions in the k space obtained from the three models given in Fig. 1 with $\eta_i = 3.0$ and $T_e/T_i = 1.0$. Fig. 2(a) is the eigenfunction $\phi(k)$ in sheared slab for $L_n/L_s = 0.1$, $k_y\rho_s = k_\theta\rho_s = 0.75$. Fig. 2(b) is the eigenfunction in quasi-toroidal model with $\epsilon_n = 0.2$ while the other parameters are the same as that in the slab case. The eigenfunction from Eq. (11) is shown in Fig. 2(c) with $\hat{s} = 1.0$, $q = 2.0$ and the same parameters used by the other models. The solid lines are the real part and the dotted lines the imaginary part. Here, we note that the eigenfunctions in the quasi-toroidal and sheared slab models are just the Fourier transform of the real x-space eigenfunction. The eigenfunctions in Figs. 2(b) and 2(c) are very similar to each other with a half width about $0.6\rho_s^{-1}$ while the meaning of this is different in each case. The half width of the eigenfunction in the sheared slab case is about $1\rho_s^{-1}$ which means that the slab mode has shorter wavelength than the quasi-toroidal mode in real x-space. So that the toroidal effect can significantly increase the transport induced by the η_i-mode turbulence when estimated with the mixing length theory as given in Refs. 7 and 22.

The growth rate and real frequency versus $k_\theta\,\rho_s$ are given in Fig. 3 for different η_i values. Again the differences between general toroidal (solid lines) and the quasi-toroidal approximation (dotted lines) are limited. The maximum growth rates are found at $k_\theta\,\rho_s \sim 0.7$ indicating that small $k_\theta\,\rho_s$ expansion is not adequate and the full integral formalism is necessary for these parameters. The growth rate and real frequency for different ϵ_n values are given in Fig. 4 as function of $k_\theta\,\rho_s$. The maximum growth rates appear at $k_\theta\,\rho_s \sim 0.7$ just as it does in Fig. 3. Note that the real frequency and growth rate are normalized to $\omega_{*e}(k_\theta\,\rho_s)^{-1} = c_s/L_n$ in Figs. 3, 4, and 5.

2. ϵ_n variation

In Fig. 5 the mode growth rate and real frequency are given as function of ϵ_n for different $k_\theta \rho_s$ values. Here, we consider only the ϵ_n effect coming from the toroidal curvature drift term ω_D, and $L_n/L_s = \hat{s}\epsilon_n/q = 0.1$ is fixed. In order to compare with quasi-toroidal model, $q = 1.5$ is fixed and $\hat{s}$ varies according to $L_n/L_s = \hat{s}\epsilon_n/q = 0.1$ in the general ballooning model (solid lines). It is easy to see that the mode real frequency increases significantly with the increasing of ϵ_n. The maximum growth rates occur around $\epsilon_n \simeq 0.2$ where the quasi-toroidal approximation is good for general toroidal dynamics. Fig. 5 can also be viewed as a normalized frequency and growth rate versus $\hat{s} \sim \frac{1}{\epsilon_n}$. In this way it seems that mode coupling has a stronger destabilizing effect when the $\hat{s}$ value is higher as expected. As an alternative, the results for fixed $\hat{s} = 1.0$ and varying q such that $L_n/L_s = \hat{s}\epsilon_n/q = 0.1$ are given (dashed line) when $k_\theta \rho_s = 0.5$. Such a choice does not change the result very much.

The mode growth rate and real frequency versus ϵ_n are given in Fig. 6 for fixed $\hat{s} = 1.0$ and given q values (in Fig. 5 $\hat{s}$ or q varies when ϵ_n changes) for general toroidal model. It is obtained that the mode real frequency increases up to $-1.3\omega_{*e}$ with the increasing $\epsilon_n \sim 0.5$ while the mode moves to the electron diamagnetic drift direction for $\epsilon_n \lesssim 0.06$. The maximum mode growth rate in this case is much higher than that in Fig. 5. This is reasonable since in Fig. 5 $\hat{s}$ increases when ϵ_n decreases in order to keep L_n/L_s constant.

From Fig. 6 it is seen that the mode growth rate increases with q when other parameters are the same. The increase of q separates the favorable and the unfavorable magnetic curvature regions making the localization of the mode to the bad curvature region more complete, leading to higher mode growth rate and transport.

3. Shear variation

The shear variation effect is shown in Fig. 7. The mode real frequency increases with shear increasing for $\hat{s} \lesssim 1$ then keeps constant for $\hat{s} > 1$. At the same time the mode growth rate increases with $\hat{s}$ increasing for $\hat{s} \lesssim 0.5$ then decreases for $\hat{s} \gtrsim 0.5$. For the region $1 < \hat{s} < 2$ the growth rate decreases as $1/\hat{s}$.

4. T_i variation at fixed T_e

The effect of increasing T_i at fixed T_e is studied in Fig. 8. The real frequency increases approximately linearly with T_i increasing. For $\epsilon_n = 0.15$ the real frequency becomes positive (rotation in the electron direction) when T_i is low ($T_i \leq 0.25\ T_e$). The mode growth rate has maximum around $T_i \sim (0.5 - 1)T_e$. For $T_e/T_i \geq 2$ the mode width $\Delta\theta \gtrsim \pi/2$ so that the mode coupling destabilizing effect seems significant when shear is high enough (low ϵ_n for fixed q and L_n/L_s). For $T_e/T_i \leq 0.8$, $\epsilon_n = 0.15$, the mode width $\Delta\theta \leq \pi/3$ and the mode coupling destabilizing effect is weak (Fig. 8(c)). This change of the mode width with T_e/T_i may explain the fact that the mode growth rate from general toroidal calculation is higher than that from the quasi-toroidal approximation for $T_e/T_i \geq 2$ while it is lower than that from the quasi-toroidal for $T_e/T_i \leq 0.8$ when $\epsilon_n = 0.15$ in Fig. 8(a).

5. T_e variation at fixed T_i

The normalized mode frequency and growth rate (normalized to $-\omega_{*i} = \omega_{*e}T_i/T_e$) are given in Fig. 9 as function of T_e/T_i to show the T_e effect when T_i is fixed. In contrast to Fig. 8 where the mode real frequency decreases when T_e/T_i increases, the mode frequency increases when T_e/T_i increases. The behavior of the growth rate is similar to that in Fig. 8 except that the maximum growth rate shifts to higher T_e/T_i and decreases much faster in Fig. 9. It seems necessary to distinguish T_e or T_i changing when T_e/T_i effect is considered. Especially,

the behavior of the real frequency may be used to define the η_i-mode turbulence from the others in experiments.

6. Local kinetic model

The comparison between general toroidal model and the local kinetic approximation is given in Fig. 10. For $k_\theta \rho_s \sim 1$ the results from these two models are very close while the integral equation gives much higher growth rates when $k_\theta \rho_s \lesssim 0.5$.

The comparison between the general toroidal model (Eq. (11)) and the quasi-toroidal model (Eq. (18)) can not be made too precisely because there is one more parameter could be chosen freely in the former than in the latter. Generally speaking, the quasi-toroidal approximation overestimates the driving force of curvature and magnetic gradient drifts (by taking $\theta = 0$) and gives higher growth rate. However, mode coupling which is considered only in the general toroidal model has a strong destabilizing effect when the mode width $\Delta\theta$ is large enough and shear is high ($\hat{s} \gtrsim 1.0$). In such cases the growth rate given by the toroidal model is about 10% to 20% higher than that given by the quasi-toroidal approximation. It has never appeared that the mode growth rate obtained from toroidal equation is much higher than the growth rate obtained from the quasi-toroidal approximation.

IV. Remarks and Discussions

A new integral equation describing the linear dynamics of low frequency perturbations such as the η_i mode in toroidal geometry is developed. The integral equation takes into account the ion drift motion due to the curvature and magnetic gradient, the effect of finite Larmor radius and the arbitrary ratio of $k_\parallel v_t/\omega_D$. Ion bounce motion is neglected, and the electrons are taken as adiabatic for simplicity. Under these conditions the integral equation is the most general equation.[8] In addition the new formalism of the integral equation has some

characteristics which allow the equation to be solved within reasonable computer time ($\sim$ 3 min/eigenvalue on the Cray-2) .

The equation is solved for a wide range of tokamak plasma parameters without further approximation. It can be concluded from the calculations that the real frequency and growth rate of η_i-mode in toroidal geometry are significantly different from the sheared slab η_i-mode. Toroidicity effects must be taken into account in the effort to connect theoretical results of the η_i-mode analysis with experimental observations in tokamaks. The numerical results presented in this work can be used to check the validity of various approximation approaches and may be compared with experimental observations. A numerical table of the complex eigenvalue over the parameter variation considered is being made available on a public domain file or on a disk available upon request.

By using the ballooning mode representation the mode coupling introduced due to the toroidal feature of the equilibrium magnetic configuration is taken into account. It is shown that the mode coupling has a strong destabilizing effect especially when mode width $\Delta\theta \geq \pi/2$ and magnetic shear $\hat{s} \geq 1$ due to the geodesic curvature effect from $\hat{s}\theta \sin\theta$ term in Eq. (5).

It is worth mentioning that the real frequency of the mode for $\epsilon_n = 0.4$ is about one order of magnitude higher than the corresponding sheared slab mode frequency (see Fig. 1(b)). The low theoretical mode frequencies of previous ITG models are claimed to be too low to explain the ion feature observed on TEXT drift wave fluctuation spectrum.[23] The increase in the mode frequency from the toroidal effect is in the right direction at least in this respect.

In addition it is claimed that ion energy transport coefficients obtained from kinetic η_i mode quasilinear theories are lower than experimental measurements.[7,11] It is shown in this work that the η_i mode growth rate in toroidal geometry is much higher than in the sheared slab, for example, the growth rate for $\epsilon_n = 0.4$ is about 3 times the value of the sheared slab mode when $\eta_i = 3.0$ (see Fig. 1(a)). At the same time the mode width in x-space for

the toroidal geometry is about twice the value of the sheared slab mode width (see Fig. 2). This increase of $\gamma(\Delta x)^2$ is in the dir ion for solving the discrepancy between the η_i mode theory and the experimental observations concerning the anomalous ion energy transport. The mode growth rate decreases with ϵ_n increasing for $\epsilon_n \gtrsim 0.2$. This qualitatively agrees with the confinement improvement in H-mode discharges which have rather large value of L_n. Detailed calculation using experimental data and comparison with observed results are underway and will be published separately. It is also straightforward to couple trapped electron and impurity effects into Eq. (11) and such work is in progress.

Acknowledgments

The authors would like to thank Dr. Y.Z. Zhang for helpful discussions. This work was supported by the U.S. Department of Energy contract DE-FG05-80ET-53088.

References

1. M. Greenwald, D.Q. Winn, S. Milora, R. Parker, and S. Wolfe, Phys. Rev. Lett. **53**, 352 (1984).

2. F.X. Sölder, E.R. Müller, F. Wagner, H.S. Bosch, A. Eberhagen, H.V. Fahrbach, G. Fussmann, O. Ghre, K. Gentle, J. Gernhardt, O. Gruber, W. Herrmann, G. Janeschitz, M. Kornherr, K. Krieger, H.M. Mayer, K. McCormick, H.D. Murmann, J. Neuhauser, R. Nolte, W. Poschenreider, H. Röhr, H.-H. Steuer, U. Stroth, N. Tsois, and H. Verbeek, Phys. Rev. Lett. **61**, 1105 (1988).

3. R.J. Fonk, R. Howell, K. Jaehnig, L. Roquemore, G. Schilling, S. Scott, M.C. Zarnstorff, C. Bush, R. Goldston, H. Hsuan, D. Johnson, A. Ramsey, J. Schivell, and H. Towner, Phys. Rev. Lett. **63**, 520 (1989).

4. S.D. Scott, P.H. Diamond, R.J. Fonck, R.B. Howell, K.P. Jahnig, G. Schilling, E.J. Synakowski, M.C. Zarnstroff, C.E. Bush, E. Fredrickson, K.W. Hill, A.C. Janos, D.K. Mansfield, D.K. Owens, H. Park, G. Pautasso, A.T. Ramsey, J. Schivell, G.D. Tait, W.M. Tang, and G. Taylor, Phys. Rev. Lett. **64**, 531 (1990).

5. D.L. Brower, W.A. Peebles, S.K. Kim, N.C. Luhmann, W.M. Tang, and P.E. Phillips, Phys. Rev. Lett. **59**, 48 (1987).

6. A.J. Wootton, Turbulence and Transport, FRCR#393, Fusion Research Center, The University of Texas at Austin, Austin, TX 78712, August, 1991.

7. W. Horton, D. Lindberg, J.-Y. Kim, J.Q. Dong, G.W. Hammett, S.D. Scott, M.C. Zarnstorff, and S. Hamaguchi, Ion Temperature Gradient Driven Transport in a Density Modification Experiment on the TFTR Tokamak, IFSR#501, Institute for Fusion Studies, The University of Texas at Austin, Austin, TX 78712, July, 1991.

8. F. Romanelli, Phys. Fluids B **1**, 1018 (1989).

9. T.S. Hahm and W.M. Tang, Phys. Fluids B **1**, 1185 (1989).

10. J.Q. Dong, P.N. Guzdar, and Y.C. Lee, Phys. Fluids **30**, 2694 (1987).

11. M. Kotschenreuther, H.L. Berk, R. Denton, S. Hamaguchi, W. Horton, C.-B. Kim, M. Lebrun, P. Lyster, S. Mahajan, W.H. Miner, P.J. Morrison, D. Ross, T. Tajima, J.B. Taylor, P.M. Valanju, H.V. Wong, S.Y. Xiao, and Y.-Z. Zhang, IAEA-CN-53, October 1990.

12. W. Horton, B.-G. Hong, and W.M. Tang, Phys. Fluids **31**, 2971 (1988).

13. S. Hamaguchi and W. Horton, Phys. Fluids B **2**, 3040 (1990).

14. L. Chen, S. Briguglio, and F. Romanelli, Phys. Fluids B **3**, 611 (1991).

15. R.R. Dominguez and M.N. Rosenbluth, Nucl. Fusion **29**, 844 (1989).

16. J.-Y. Kim and W. Horton, Phys. Fluids B **3**, 1167 (1991).

17. C.Z. Cheng and K.T. Tsang, Nucl. Fusion **21**, 643 (1981).

18. P.N. Guzdar, L. Chen, W.M. Tang, and P.H. Rutherford, Phys. Fluids **26**, 673 (1983).

19. X.Q. Xu and M.N. Rosenbluth, Phys. Fluids B **3**, 627 (1991).

20. Y.C. Lee, J. Van Dam, and A. Glasser, in "Finite Beta Theory" (Proc Workshop, Washington, DC, 1977), Conf-7709167, U.S. Department of Energy, Washington, DC (1977).

21. R. Courant and D. Hilbert, Methods of Mathematical Physics (Interscience, New York, 1953) Vol. 1, p. 112.

22. B.-G. Hong and W. Horton, Phys. Fluids B **2**, 978 (1990).

23. W.A. Peebles, D.L. Brower, R. Philipona, K. Burrell, R. Bravenec, E.J. Doyle, R. Groebner, N.C. Luhmann, Jr., H. Matsumoto, C. Retig, B.A. Smith, C.X. Yu, R.P. Seraydarian, Z.M. Zhang, and the DIII-D/TEXT Research Groups, N. Bretz, A. Cavallo, R.J. Fonck, T.S. Hahm, E. Mazzucato, R. Nazikian, S.F. Paul, G. Rewoldt, D.R. Roberts, W.M. Tang, G. Taylor, and the TFTR Research Group, IAEA-CN-53/A-7-12, 1990.

Figure Captions

1. Normalized growth rate γ/ω_{*e} (a) and real frequency $\omega_r/\omega_{*e}(b)$ vs. η_i for $T_e/T_i = 1$, $k_\theta \rho_s = 0.75$, $L_n/L_s = 0.1$, and $\epsilon_n = 0.2$ and 0.4. The solid lines are the general toroidal with $q = 2$, and $\hat{s} = L_n q/L_s\epsilon_n$, the dotted lines are the quasi-toroidal approximation and sheared slab limit with $\epsilon_n = 0$.

2. Eigenfunctions $\widehat{\phi}(k)$ in the k-space for the three cases of Fig. 1 with $\eta_i = 3.0$, (a)–the sheared slab mode; (b)–the quasi-toroidal model with $\epsilon_n = 0.2$; (c)–general toroidal model with $\hat{s} = 1.0$, $q = 2.0$. The other parameters are the same as used in Fig. 1. The solid lines are the real part and the dotted lines the imaginary part.

3. Normalized growth rate $\gamma L_n/c_s = \gamma\, k_\theta\, \rho_s/\omega_{*e}$ (a) and real frequency (b) $\omega_r L_n/c_s$ vs. $k_\theta\, \rho_s$ for $\eta_i = 1.5, 2, 3$ when $T_e/T_i = 1$, $L_n/L_s = 0.1$, and $\epsilon_n = 0.2$. Dotted lines correspond to quasi-toroidal approximation, and the solid lines the general toroidal results with $q = 2$ and $\hat{s} = L_n q/L_s\epsilon_n$.

4. Normalized growth rate $\gamma L_n/c_s = \gamma\, k_\theta\, \rho_s/\omega_{*e}$ (a) and real frequency (b) $\omega_r L_n/c_s$ vs. $k_\theta\, \rho_s$ for $\epsilon_n = 0.2,\ 0.3,\ 0.45$ when $T_e/T_i = 1$, $L_n/L_s = 0.1$, and $\eta_i = 2.5$. Dotted lines correspond to quasi-toroidal approximation, and the solid lines the general toroidal results with $q = 1.5$ and $\hat{s} = L_n q/L_s\epsilon_n$.

5. Normalized growth rate $\gamma L_n/c_s$ vs. ϵ_n for $k_\theta \rho_s = 0.3, 0.5, 0.7$ when $\eta_i = 2.5$, $T_e/T_i = 1$, $L_n/L_s = 0.1$. The dotted lines represent the quasi-toroidal approximation, the solid lines the general toroidal results with $q = 1.5$ and the dashed line with $\hat{s} = 1.0$.

6. Normalized growth rate γ/ω_{*e} vs. ϵ_n for $q = 1.1,\ 1.5,\ 2,\ 2.5,\ 3$ when $T_e/T_i = 1$, $\eta_i = 2.5$, $k_\theta\, \rho_s = 0.5$, $\hat{s} = 1.0$. These are the general toroidal results.

7. Normalized growth rate γ/ω_{*e} vs. $\hat{s}$ for $q = 1.5, 2.0, 2.5$ when $\eta_i = 2.5$, $T_e/T_i = 1$, $k_\theta \rho_s = 0.5$, $\epsilon_n = 0.25$. The solid lines represent the general toroidal results and the dotted lines the quasi-toroidal approximation.

8. Normalized growth rate γ/ω_{*e} (a) and real frequency ω_r/ω_{*e} (b) vs. T_e/T_i (T_e = constant) for various values of ϵ_n when $k_\theta \rho_s = 0.7$, $L_n/L_s = 0.1$, $\eta_i = 2.5$. The dotted lines represent the quasi-toroidal approximation and the solid lines the general toroidal results where $q = 1.5$ and $\hat{s} = L_n q/L_s \epsilon_n$ are used. (c) The eigenfunctions $\hat{\phi}(\theta)$ for $\epsilon_n = 0.15$.

9. Normalized growth rate $\gamma/|\omega_{*i}|$ (a) and mode frequency $\omega_r/|\omega_{*i}|$ (b) versus T_e/T_i (T_i = constant) for $\eta_i = 2.5$, $k_\theta \rho_s = 0.70$ and $q = 1.5$. These are the general toroidal results.

10. Normalized growth rate $\gamma L_n/c_s = \gamma\, k_\theta\, \rho_s/\omega_{*e}$ (a) and real frequency (b) $\omega_r L_n/c_s$ vs. $k_\theta\, \rho_s$ for $q = 1.5,\ 2.0,\ 2.5$ when $T_e/T_i = 1$, $\epsilon_n = 0.25$, $\hat{s} = 0.6$ and $\eta_i = 2.5$. Dotted lines correspond to local kinetic approximation where $k_{||} = 1/qR$ is used, and the solid lines the general toroidal results.

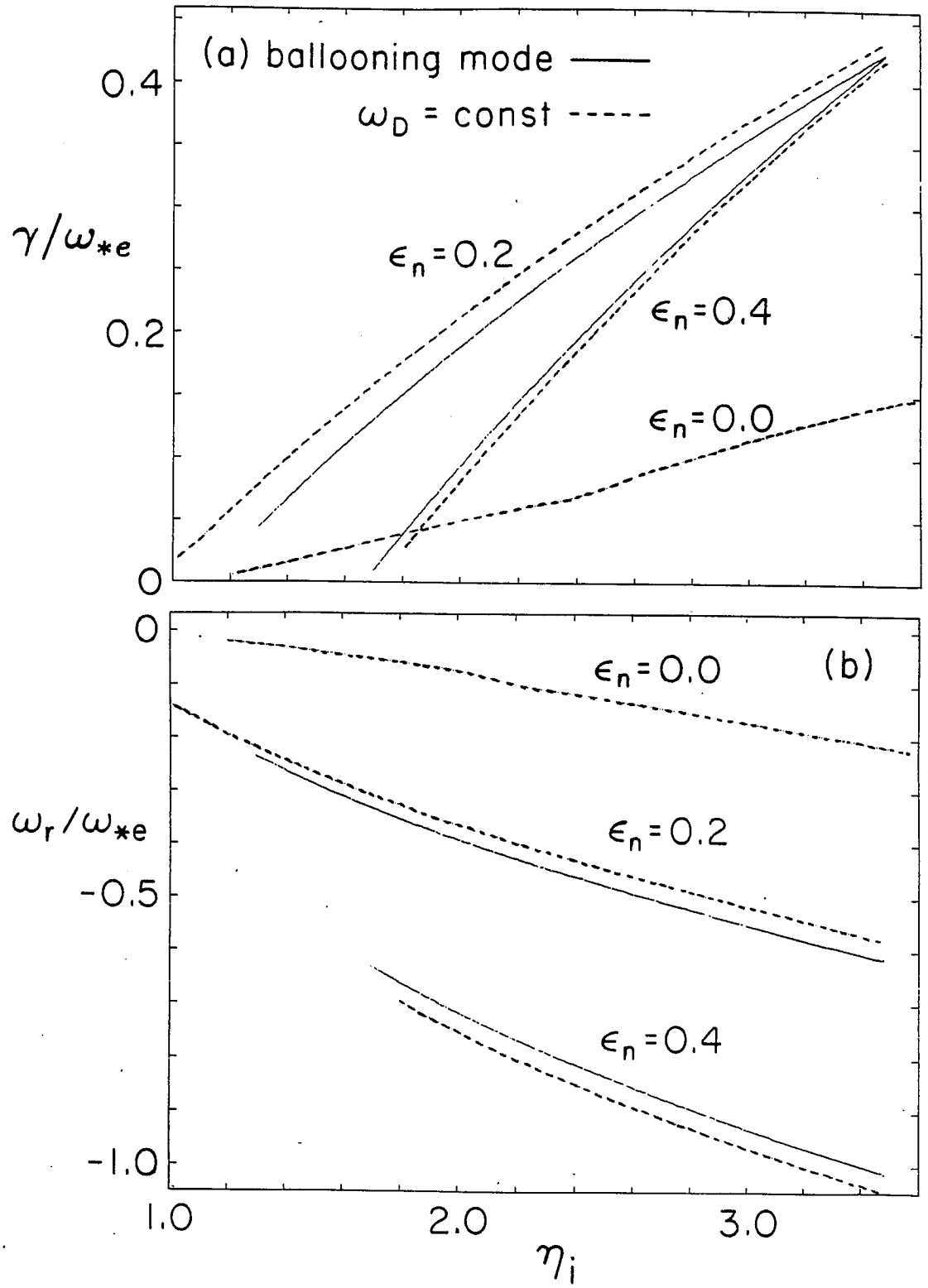
(a) ballooning mode
ω_D = const
ϵ_n=0.2
ϵ_n=0.4
ϵ_n=0.0
γ/ω_{*e}
0.4
0.2
0
(b)
ϵ_n=0.0
ϵ_n=0.2
ϵ_n=0.4
ω_r/ω_{*e}
-0.5
-1.0
1.0
2.0
3.0
η_i

Fig.1

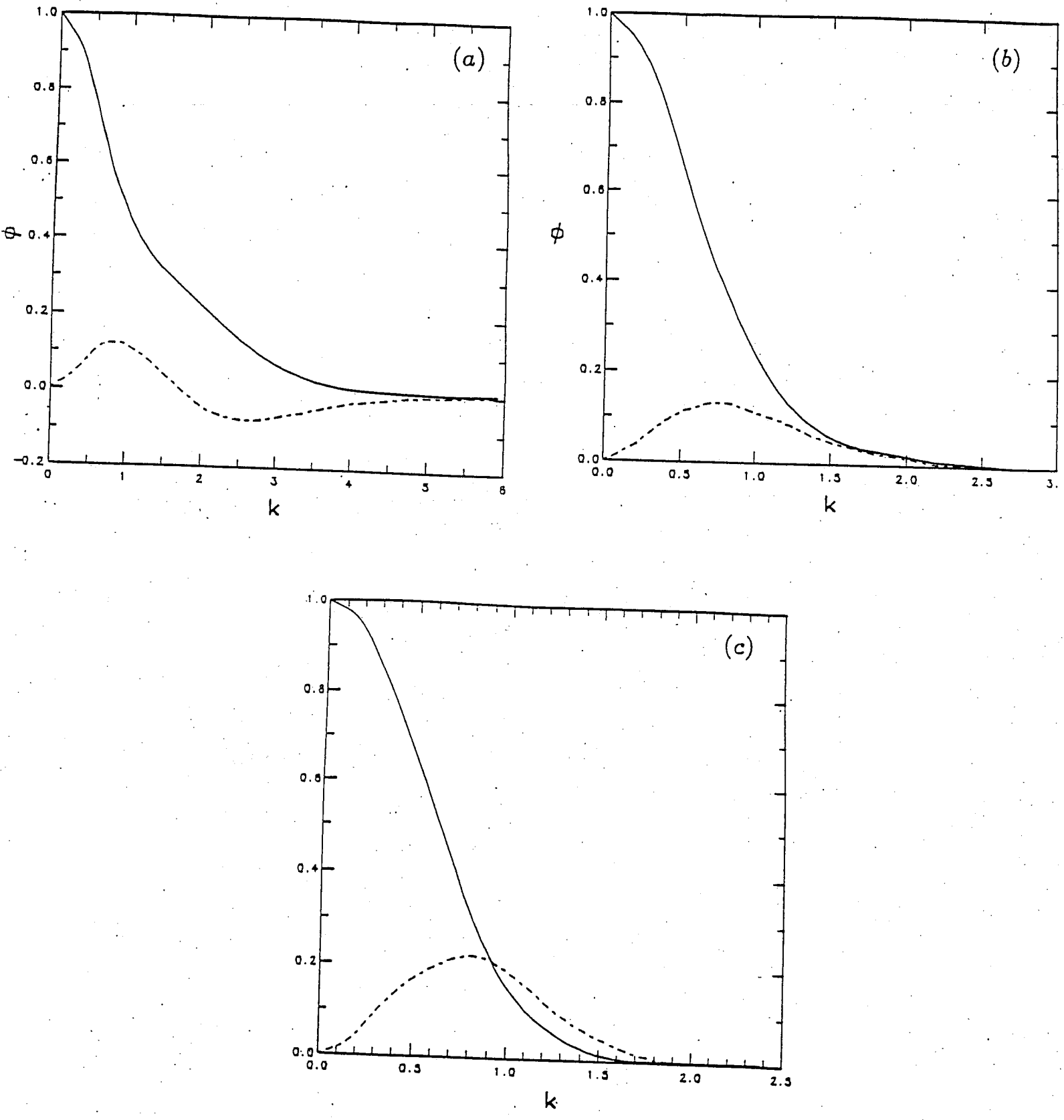

Fig.2

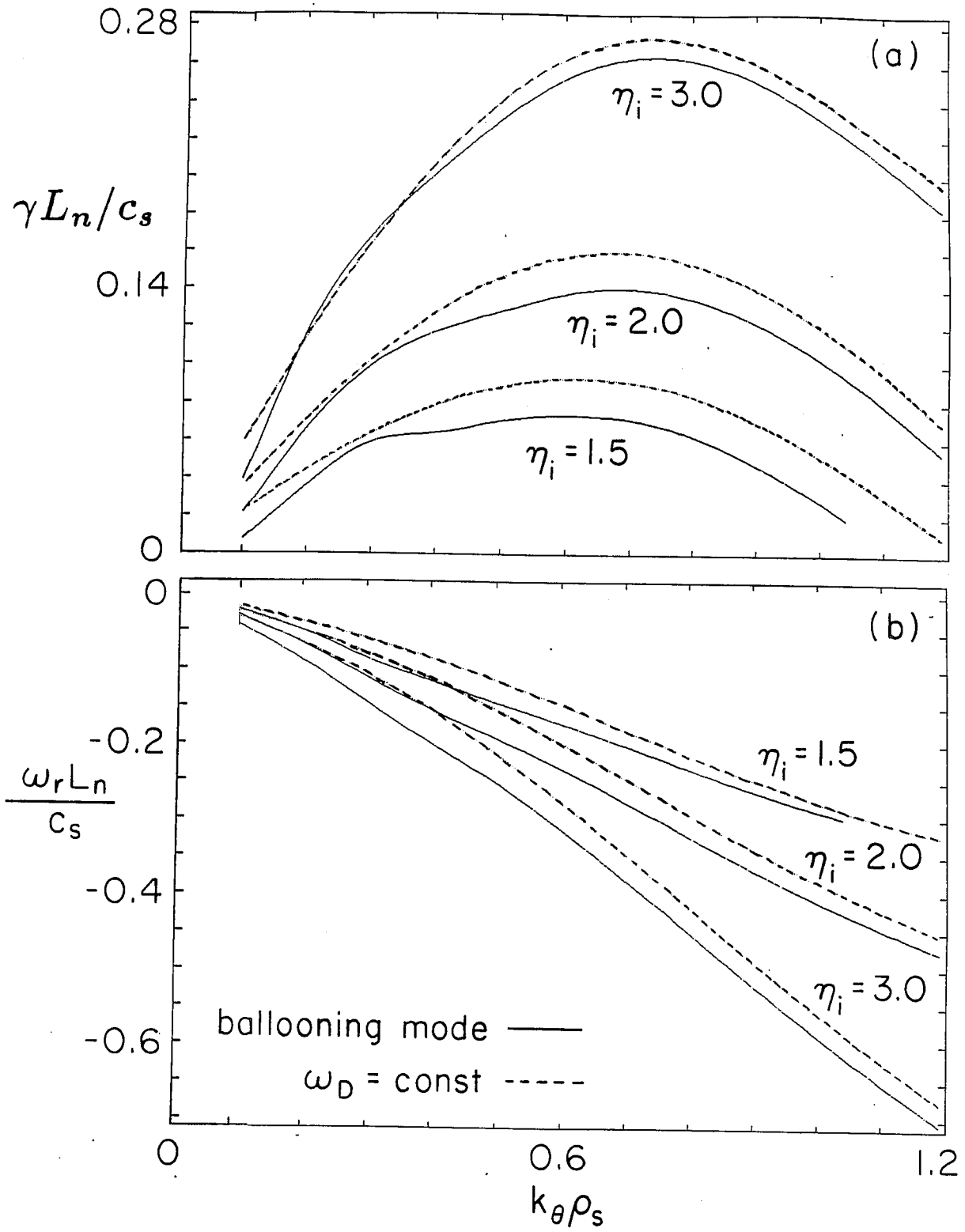
0.28
0.14
0
$\gamma L_n/c_s$
(a)
$\eta_i = 3.0$
$\eta_i = 2.0$
$\eta_i = 1.5$
0
-0.2
-0.4
-0.6
$\frac{\omega_r L_n}{c_s}$
(b)
$\eta_i = 1.5$
$\eta_i = 2.0$
$\eta_i = 3.0$
ballooning mode
ω_D = const
0
0.6
1.2
$k_\theta \rho_s$

Fig.3

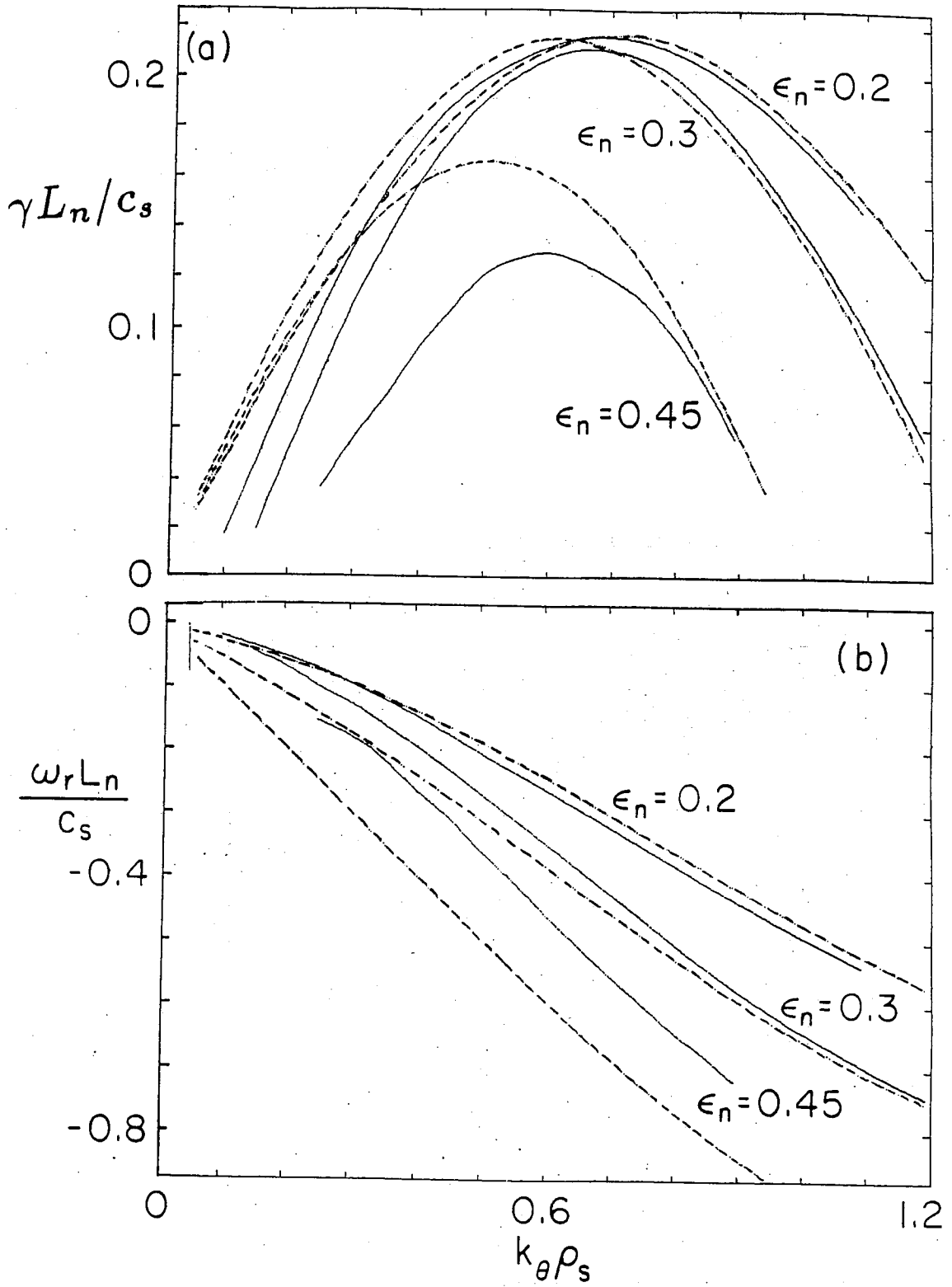
(a)
0.2
0.1
0
$\gamma L_n/c_s$
ϵ_n=0.2
ϵ_n=0.3
ϵ_n=0.45
(b)
0
-0.4
-0.8
$\frac{\omega_r L_n}{c_s}$
ϵ_n=0.2
ϵ_n=0.3
ϵ_n=0.45
0
0.6
1.2
$k_\theta \rho_s$

Fig.4

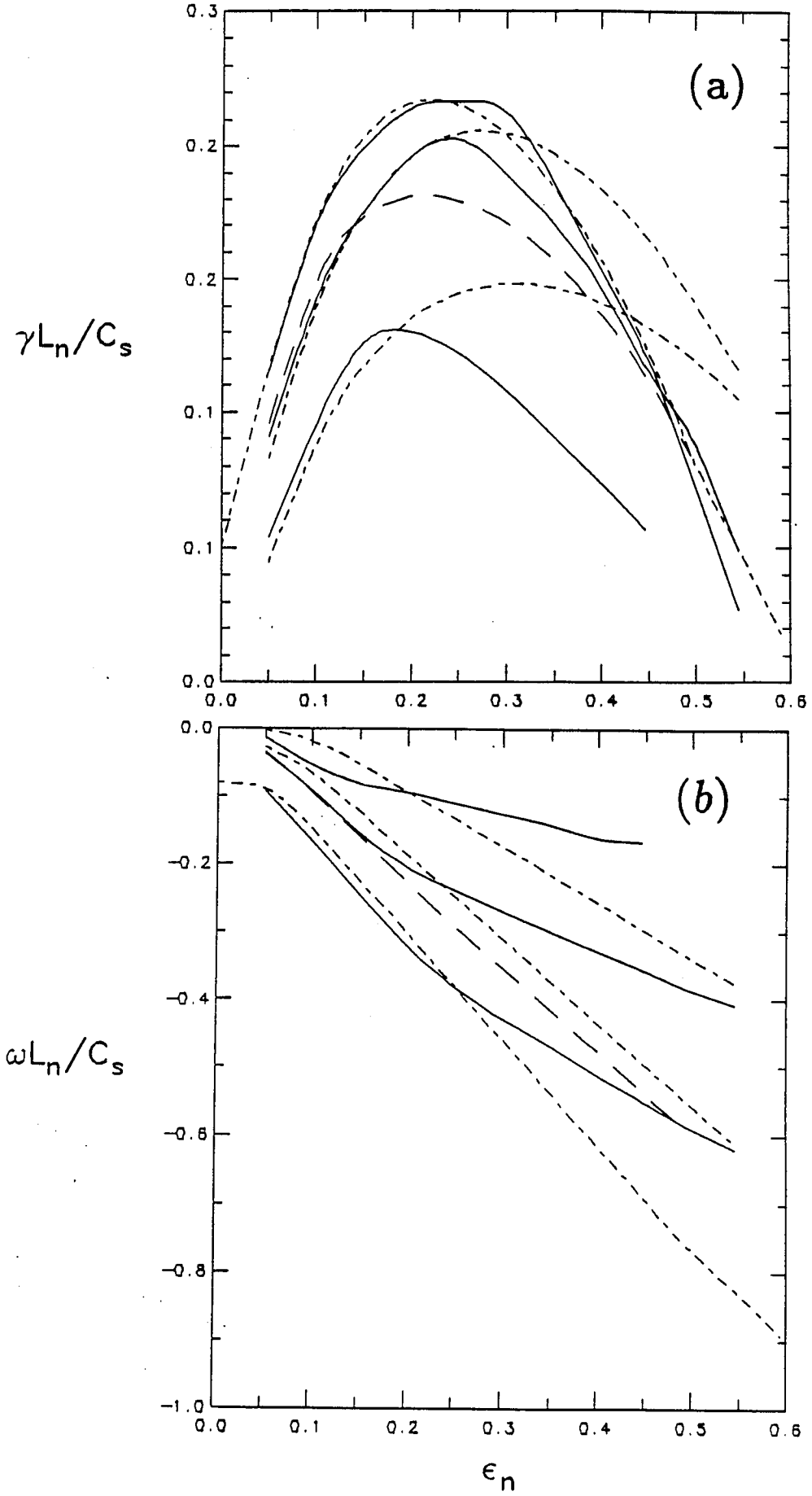
(a)
(b)
$\gamma L_n/C_s$
$\omega L_n/C_s$
ϵ_n
0.3
0.2
0.2
0.1
0.1
0.0
0.0
0.1
0.2
0.3
0.4
0.5
0.6
0.0
−0.2
−0.4
−0.6
−0.8
−1.0

Fig.5

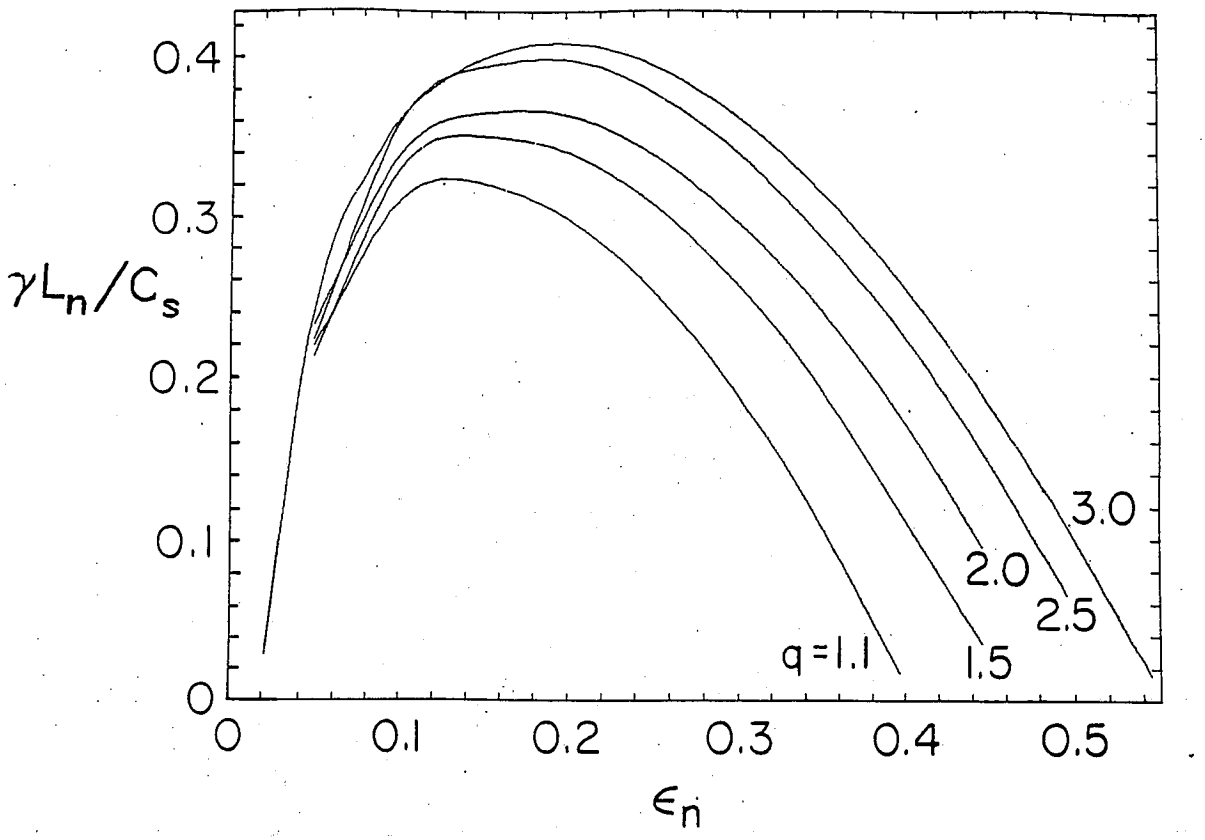

Fig.6

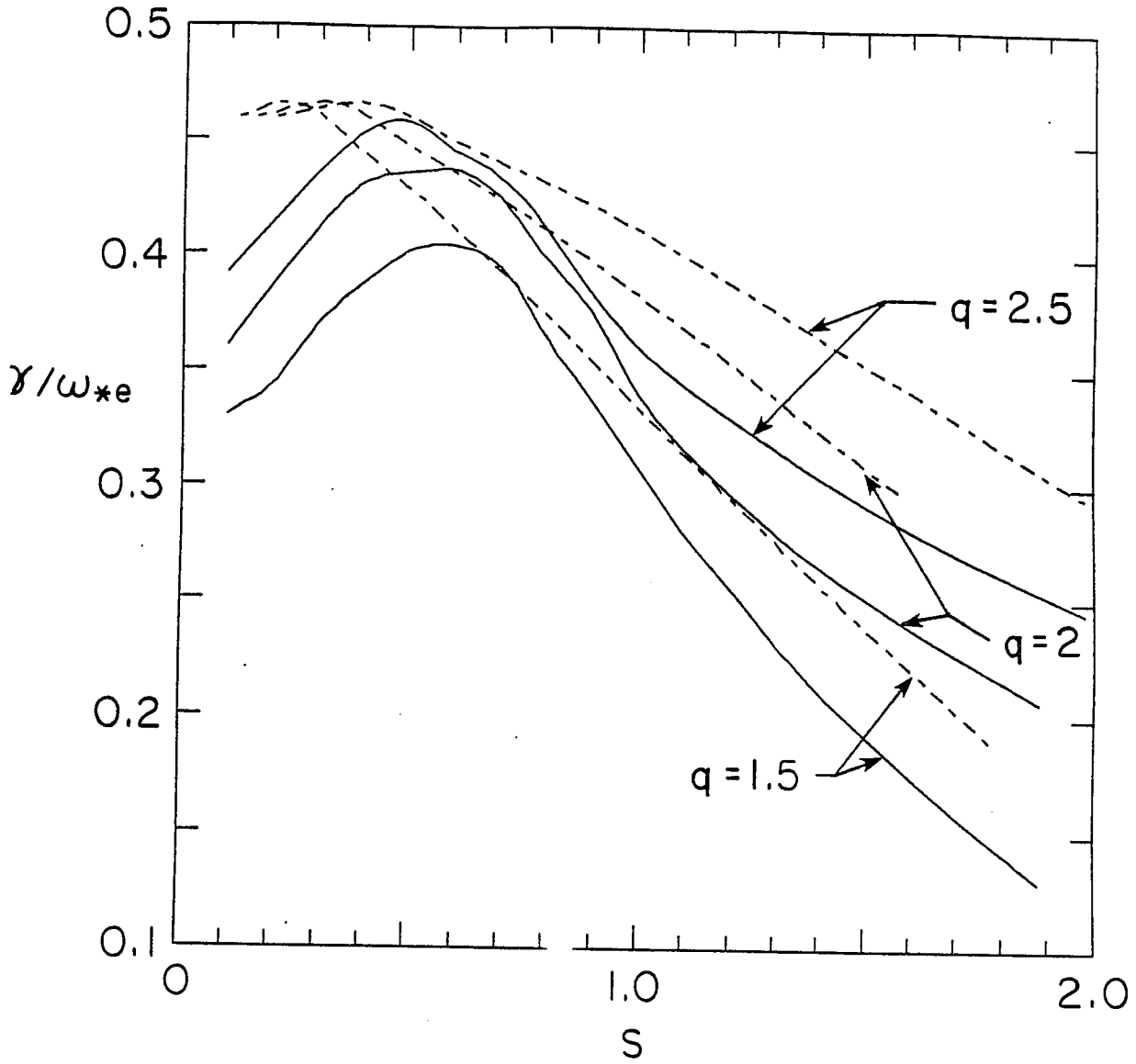

Fig.7

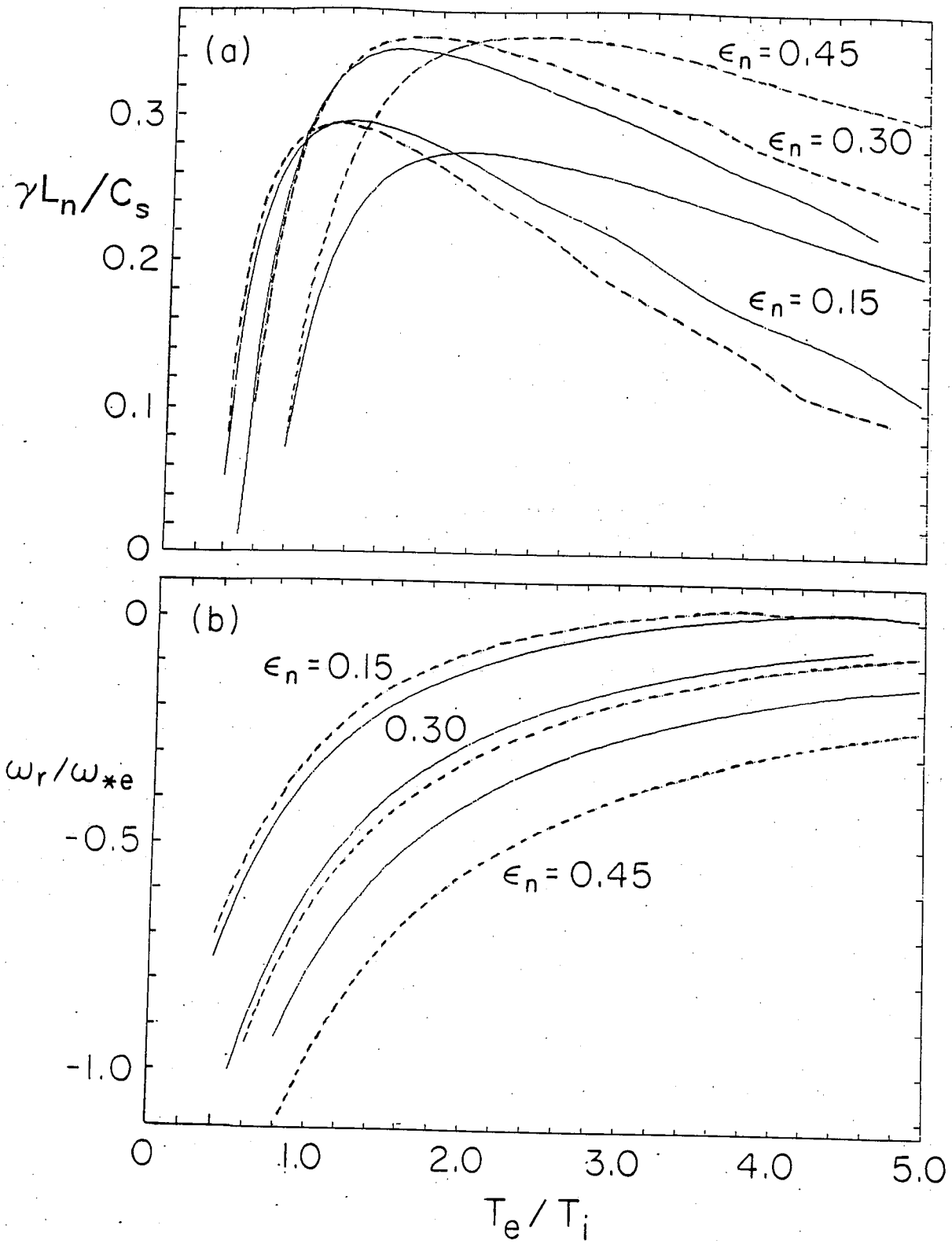
(a)
$\epsilon_n = 0.45$
$\epsilon_n = 0.30$
$\epsilon_n = 0.15$
$\gamma L_n / C_s$
0.3
0.2
0.1
0
(b)
$\epsilon_n = 0.15$
0.30
$\epsilon_n = 0.45$
ω_r / ω_{*e}
0
-0.5
-1.0
0
1.0
2.0
3.0
4.0
5.0
T_e / T_i

Fig.8

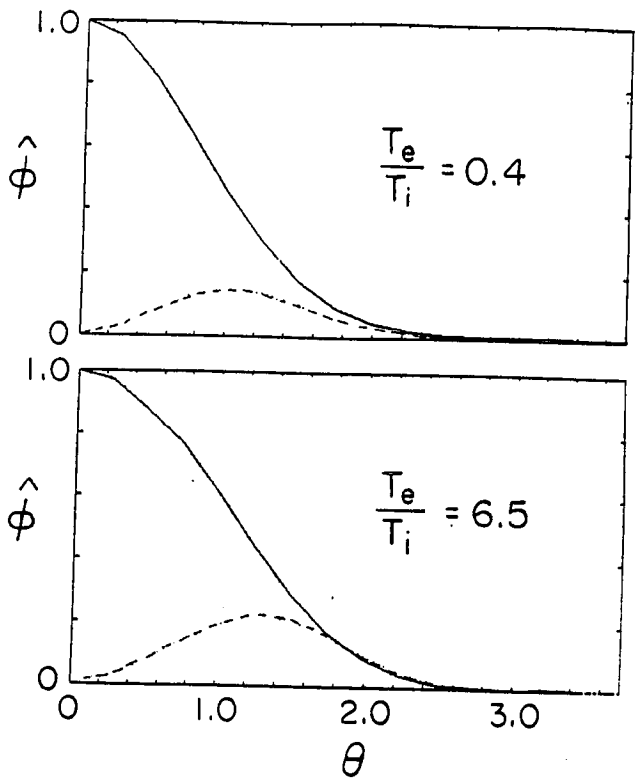
1.0
$\hat{\phi}$
$\frac{T_e}{T_i}$ = 0.4
0
1.0
$\hat{\phi}$
$\frac{T_e}{T_i}$ = 6.5
0
0
1.0
2.0
3.0
θ

Fig.8 (c)

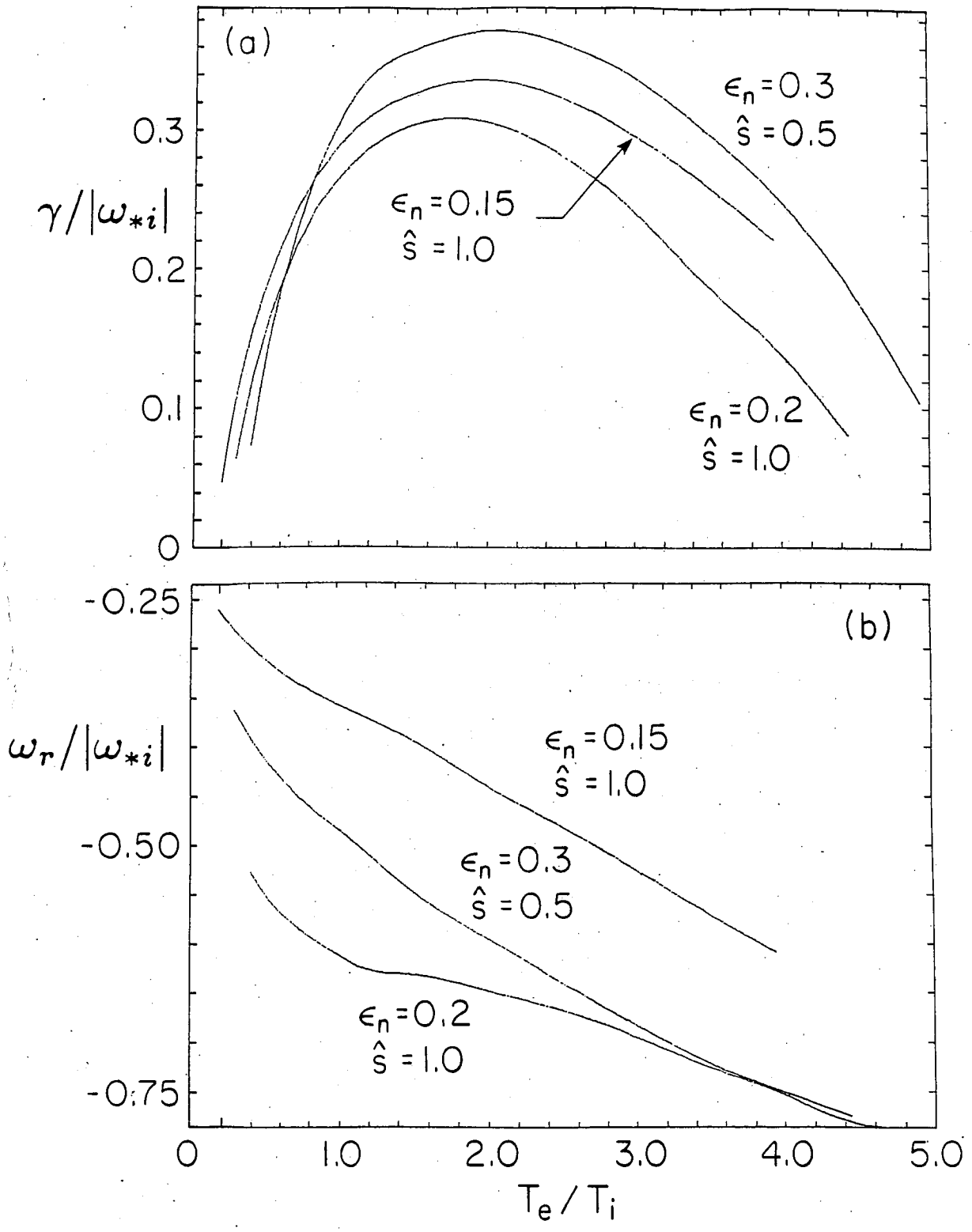
(a)
$\epsilon_n = 0.3$
$\hat{s} = 0.5$
$\epsilon_n = 0.15$
$\hat{s} = 1.0$
$\epsilon_n = 0.2$
$\hat{s} = 1.0$
$\gamma/|\omega_{*i}|$
0.3
0.2
0.1
0
(b)
$\omega_r/|\omega_{*i}|$
-0.25
-0.50
-0.75
$\epsilon_n = 0.15$
$\hat{s} = 1.0$
$\epsilon_n = 0.3$
$\hat{s} = 0.5$
$\epsilon_n = 0.2$
$\hat{s} = 1.0$
0
1.0
2.0
3.0
4.0
5.0
T_e / T_i

Fig.9

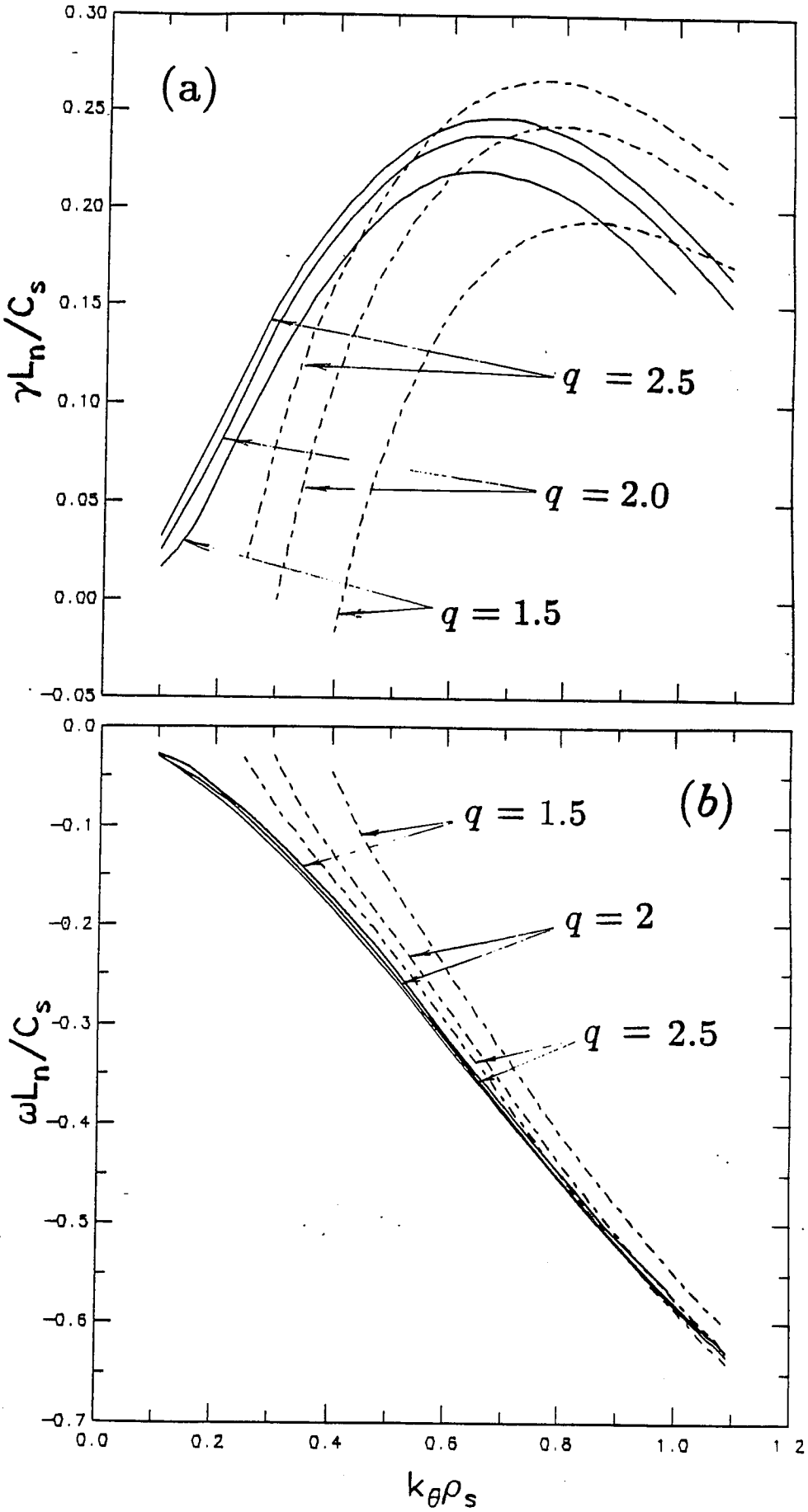

Fig.10